ADVANCED ENERGY MATERIALS
www.advenergymat.de

Iodine Modulates the MACl-Assisted Growth of $FAPbI_3$ for High Efficiency Perovskite Solar Cells

Junnan Hu, Jae Won Ahn, Zhaojian Xu, Min Ju Jeong, Chanhyeok Kim, Jun Hong Noh, Hanul Min,* and Barry P. Rand**

The preferential growth of α-phase formamidinium perovskite (α-$FAPbI_3$) at low temperatures can be achieved with the incorporation of chloride-based additives, with methylammonium chloride (MACl) being the most common example. However, compared to other less-volatile chloride additives, MACl only remains in the growing perovskite film for a short time before evaporating during annealing, primarily influencing the early stages of film formation. In addition, evaporation of MACl as methylamine (MA^0) and HCl can introduce a side reaction between MA^0 and formamidinium (FA), undermining the compositional purity and phase stability of α-$FAPbI_3$. In this study, it is demonstrated that addition of iodine (I_2) into the $FAPbI_3$ precursor solution containing MACl suppresses the MA-FA side reaction during annealing. Additionally, MACl evaporation is delayed owing to strong interaction with triiodide. The added I_2 facilitates spontaneous growth of α-$FAPbI_3$ prior to annealing, with an improved bottom morphology due to the formation of fewer byproducts. Perovskite solar cells derived from an I_2-incorporated solution deliver a champion power conversion efficiency of 25.2% that is attributed to suppressed non-radiative recombination.

1. Introduction

Chloride-based additives have been widely employed in processing high quality perovskite films, with methylammonium chloride (MACl) among the most common choices in high efficiency formamidinium (FA)-based perovskite solar cells (PSCs).[1–4] The addition of MACl to the perovskite precursor solution has been correlated to improved crystallinity and morphology with a preferential growth of the visible-light-absorbing α-phase formamidinium perovskite (α-$FAPbI_3$) at low annealing temperature.[5–8] The incorporation of MACl into the $FAPbI_3$ precursor solution leads to the presence of MA^+ in perovskite films at different stages of annealing, and helps to stabilize the cubic α-$FAPbI_3$ phase due to the smaller ionic size of MA^+[9]; under typical annealing conditions, the majority of MACl is ultimately removed from the film.[6] However, the volatility of MACl is detrimental in numerous ways. Compared to less volatile organoammonium chloride analogs with longer alkyl chains, MACl exits at the early stages of annealing, making it less influential in the ultimate growth of high-quality perovskite films.[10] Additionally, the loss of MA^+ involves deprotonation with the release of methylamine (MA^0) and HCl.[11] The MA^0 can react with FA^+ via an addition-elimination reaction, whereby *N*-methyl formamidinium (MFA^+) and *N,N'*-dimethyl formamidinium ($DMFA^+$) are observed to be the non-volatile reaction products.[12–15] The formation of these MA-FA adducts is problematic, because this

J. Hu, Z. Xu, B. P. Rand
Department of Electrical and Computer Engineering
Princeton University
Princeton, NJ 08544, USA
E-mail: brand@princeton.edu
J. W. Ahn, M. J. Jeong, J. H. Noh
School of Civil
Environmental and Architectural Engineering
Korea University
Seoul 02841, Republic of Korea
E-mail: junhnoh@korea.ac.kr
The ORCID identification number(s) for the author(s) of this article can be found under https://doi.org/10.1002/aenm.202400500

DOI: 10.1002/aenm.202400500

C. Kim, H. Min
KU-KIST Graduate School of Converging Science and Technology
Korea University
Seoul 02841, Republic of Korea
E-mail: hmin92@korea.ac.kr
J. H. Noh
KU-KIST Green School Graduate School of Energy and Environment
Korea University
Seoul 02841, Republic of Korea
J. H. Noh, H. Min
Department of Integrative Energy Engineering
Korea University
Seoul 02841, Republic of Korea
B. P. Rand
Andlinger Center for Energy and the Environment
Princeton University
Princeton, NJ 08544, USA

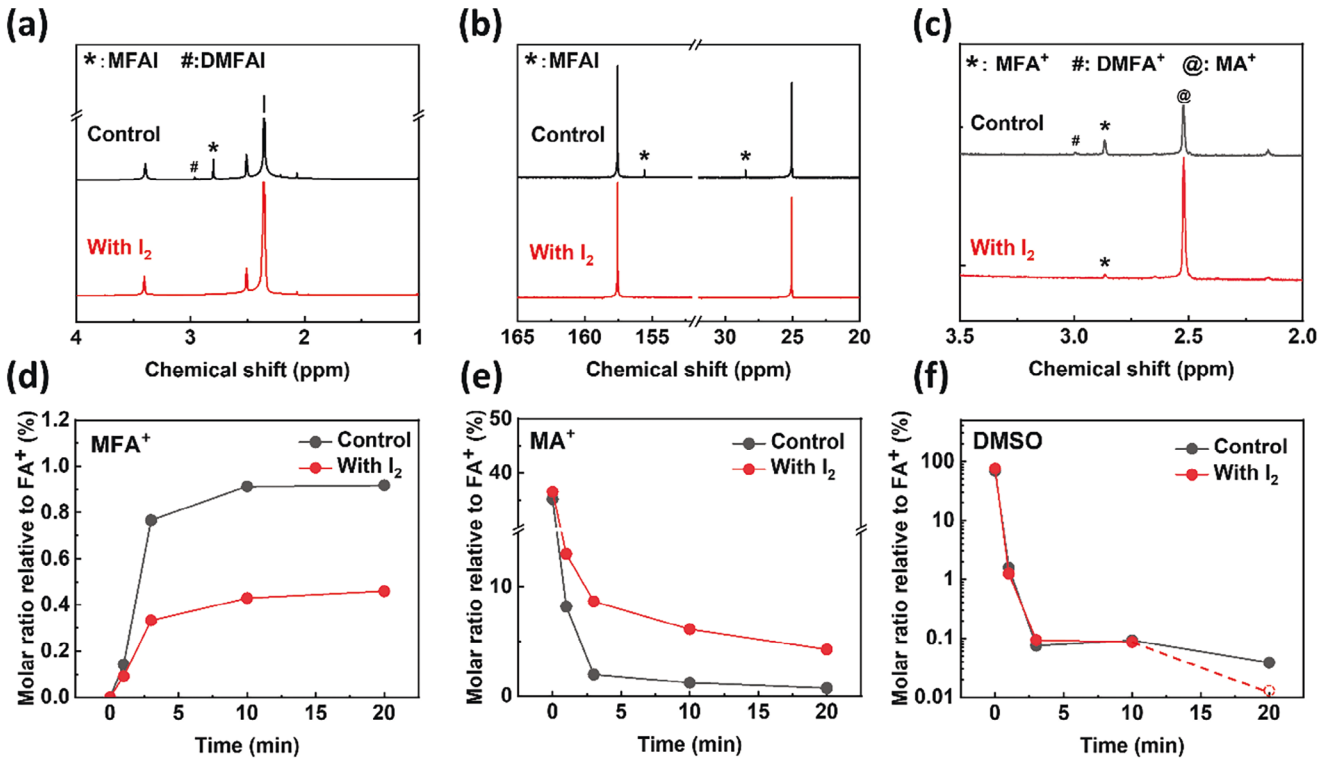

Figure 1. a) ^{1}H NMR spectra and b) ^{13}C NMR spectra of $FA_{0.5}MA_{0.5}PbI_3$ precursor solutions (in DMSO-d_6) aged in N_2 under 60 °C for 24 h; c) ^{1}H spectra of perovskite thin films (fabricated with the same recipe used for PSCs) dissolved in D_2O after annealing at 150 °C for 10 min; The evolution of d) MFA^+, e) MA^+, and f) DMSO versus annealing time in ^{1}H NMR of samples in (c). The dashed data point in (f) represents the estimated amount of DMSO in "With I_2" that is below the detection limit.

side reaction will consume FA^+ from the precursor and potentially lead to a perovskite sample with nonoptimized stoichiometry and inferior reproducibility. A recent study also revealed that MFAI can react with PbI_2 to yield trigonal $MFAPbI_3$ that is incompatible with α-$FAPbI_3$ but able to form a solid solution with δ-$FAPbI_3$ and inhibit phase transition to α-$FAPbI_3$.[16] Ultimately, we anticipate that the benefits of MACl additives can be further amplified upon mitigating their volatility and subsequent side reaction with FA.

Iodine (I_2) is generally considered to be a problematic, or at least complicated, reagent, when it comes to perovskite precursor solutions. Due to the iodide-rich environment in perovskites, presence of I_2 in the form of triiodide (I_3^-) in precursor solution indicates the oxidation of I^-, which usually leads to underperforming PSCs.[17–19] The degradation of perovskite layers under stress can also slowly release I_2 that is unfavorable for solid-state perovskites in that it induces formation of the undesired δ-$FAPbI_3$ and I_3^- facilitates the self-propagating catalytic degradation of the perovskite film.[20–23] Additionally, I_2 can migrate to transport layers or metal electrodes, further compromising device behavior and stability.[24–26] Numerous efforts have thus been made to prevent formation of I_2, either in the perovskite precursor solution or in the solid-state perovskite film. That being said, there are limited reports of the addition of I_2 to the precursor solution. One notable example was the addition of I_2 to a mixed alkylammonium salt isopropyl alcohol (IPA) solution in a two-step process that resulted in record PSCs at the time.[27] A follow-up study showed that a similar strategy could be applied in a one-step processing approach, where a I_3^- IPA solution was added to perovskite solutions, reducing the colloidal size of iodoplumbates to achieve lowered defect density and enhanced crystallinity.[28] However, it is noteworthy that excessive I_2 (typically > 20 mmol %) is reported to result in PSCs with worse performance compared to controls.[27,28]

Here we show that the addition of I_2 to MACl-$FAPbI_3$ precursor solutions, at concentrations two orders of magnitude higher than those previously reported to be excessive, can greatly enhance the performance of $FAPbI_3$-based PSCs. We show by nuclear magnetic resonance (NMR) that the addition of I_2 suppresses the MA-FA side reaction, and the volatility of MACl is also curtailed with a delayed release of MA during annealing. Both can be attributed to the strong interaction between the alkylammonium cation and I_3^-, as further correlated to thermal gravimetric analysis (TGA). The I_2-assisted $FAPbI_3$ layers show improved crystallinity via a faster and preferential growth towards α-$FAPbI_3$. Solar cells based on these perovskite films exhibit a power conversion efficiency (PCE) over 25%.

2. Results and Discussion

The ability of I_2 to suppress the MA-FA side reaction is first examined in aged perovskite precursor solutions. **Figure 1a** shows the ^{1}H NMR spectra of $FA_{0.5}MA_{0.5}PbI_3$ precursor solutions that have been sealed and aged in N_2 at 60 °C for 24 h. The molar ratio of

MA to FA is increased from 28% in the perovskite precursor solution used for films and PSCs, to 100% here, to magnify the side reaction and facilitate characterization. Unlike the spectrum of the solution with 10 mol% added I_2 (denoted as "With I_2"), there are two extra peaks in that of the control solution centered at 2.87 and 3.00 ppm, representing the methyl protons from MFA^+ and $DMFA^+$, respectively, due to the MA-FA side reaction. This can be further verified in the ^{13}C NMR spectra as shown in Figure 1b, where the extra peaks centered at 28.49 and 155.56 ppm in the control spectrum can be assigned to the methyl and imine carbons in MFA^+, respectively. The NMR spectra of aged precursor solutions with different molar ratios of I_2 can be seen in Figure S1 (Supporting Information). Our previous study reveals that I_3^- can strongly interact with both MA^+ and FA^+ through hydrogen bonding.[22] Interestingly, the presence of triazine, which is usually observed from the degradation of aged FA-only perovskite solutions, is not observed in MA-FA mixed perovskite solutions, with or without I_2, even though our previous study suggests that I_3^- can catalyze the degradation of FA^+. We suspect that this is due to the MA-FA reaction becoming the dominant reaction in mixed MA-FA perovskite solutions attributed to the presence of MA^+ that more readily interacts with I_3^-.

The NMR experiments on aged perovskite solutions indicate that the addition of I_2 can suppress the MA-FA side reaction and potentially prolong the lifetime of precursor solutions, given that many studies have linked precursor lifetime to the degree of MA-FA reaction.[12,15] Additionally, the annealing process following initial solution casting is another form of "aging" and often employs higher temperatures than those used for ink storage or preparation, at a time when volatile species can readily leave. To further explore whether the addition of iodine can play a role during annealing, perovskite thin films were prepared using the same precursor solutions as those used for PSC fabrication. After annealing, solid-state perovskite layers were dissolved in deuterated water for NMR. As shown in Figure 1c, similar results were reproduced for solid perovskite films after annealing for 10 min at 150 °C, a common annealing temperature for PSC fabrication, where films "With I_2" show substantially lower side reaction product concentrations compared to the control. These undesired byproducts have the potential to serve as nonradiative recombination sites and compromise device performance and stability.[29] To better understand the annealing process, several key species (MFA^+, MA^+, and DMSO) in perovskite samples after various annealing times were monitored via ^1H NMR, as shown in Figure 1d–f. For a semi-quantitative analysis, NMR peak integrations are further converted to molar ratios after being calibrated to that of FA^+ that is relatively constant since FA^+ is less volatile and is the dominant species at the later stages of annealing and film formation. The complete spectra are shown in Figures S2 and S3 (Supporting Information). As depicted in Figure 1d, the amount of MFA^+, an indicator for the degree of side reaction, saturates in the control at a significantly higher level compared to that with I_2. It should be noted that the analysis for MFA^+, especially with I_2, should be considered as a rough estimate, since the MFA^+ signals are so weak that they are at the detection limit. The opposite trend is observed for MA^+ as demonstrated in Figure 1e, where the amount of MA^+ in samples with added I_2 stays at a significantly higher level during different stages of annealing compared to that in the control. Specifically, the amount of MA^+ in the film with added I_2 is ≈5 times larger than that in the control from 3 to 20 min. Besides evaporation, the MA-FA side reaction will also consume MA^+, with MFA^+ as the major side product. But the concentration of MFA^+ is always below 1%, and further suppressed by I_2 addition as discussed above. However, the distinction in MA^+ with or without I_2 is on a much larger scale compared to that of MFA^+, which can only be explained by different losses of MACl in the form of MA^0 during annealing. The difference in MA^+ indicates that the addition of I_2 retards the escape of MA^+. More initial MACl in the precursor can also keep more MACl within the film during annealing, but it will lead to substantially worse MA-FA side reaction as discussed in Figure S4 (Supporting Information). With the presence of I_2 in the precursor solution, MA^+, or MACl as a whole, is less volatile during annealing with a greater influence on modulating the growth of perovskites, presumably due to the strong interaction between MA^+ and I_3^-. The effect of I_2 addition in the precursor solution and during annealing is summarized in **Scheme 1**. The MA^+ introduced as the MACl component of the ink can produce the nucleophile MA during annealing, which can readily evaporate i) or further react with FA^+ and form MFA^+ as a side-product ii). However, the strong interaction between MA^+ and I_3^- results in an intermediate, which is relatively stable on the timescale of annealing, and slows the escape of MACl and suppresses the MA-FA side-reaction (iii).

Notably, there is no obvious variance in the amount of DMSO (Figure 1f), which has been previously linked to MA-FA side reaction by facilitating proton transfer, and thus the presence of I_2 does not influence the loss of DMSO.[29,30] However, it is observed that a high rate of MFA^+ formation coincides with a considerable presence of DMSO before 3 min. We speculate that as long as one can control the side reaction at the earliest stages of annealing when there is still a large amount of residual solvent, volatile additives like I_2 can still have large impacts to the side reaction during the entire annealing process.

The volatility of I_2 and its interaction with organoammonium halides are further explored via TGA, as shown in Figure S5 (Supporting Information). To better analyze different overlapping decomposition stages, the first derivatives of the TGA curves (differential thermogravimetric analysis, DTA), are plotted in **Figure 2a**, where the temperature range is focused on the weight loss relevant to I_2 (full data set can be seen in Figure S6, Supporting Information). The valleys observed in the DTA curves correspond to the temperature of maximum weight loss rate (T_{max}), directly reflecting the I_2 volatility under various conditions. It could also be a crucial indicator for the interaction associated with I_2. As a baseline for these measurements, it is noted that T_{max} for I_2 is at 143 °C, which is close to the typical annealing temperatures for FA-based perovskite films. We also note that the curve for an MACl-I_2 mixture shows a pattern reminiscent of a combination of I_2 and MACl. However, the profiles for MAI-I_2 and FAI-I_2 mixtures differ significantly, with loss of I_2 impeded until elevated temperatures. In detail, MAI-I_2 exhibits a basin starting at ≈200 °C that is beyond typical perovskite annealing temperatures. There is no obvious T_{max} for FAI-I_2, but the weight loss below 200 °C is also negligible. Interestingly, the curve of MACl-FAI-I_2 exhibits similar features to that of MAI-I_2 with similarly delayed T_{max}, suggesting

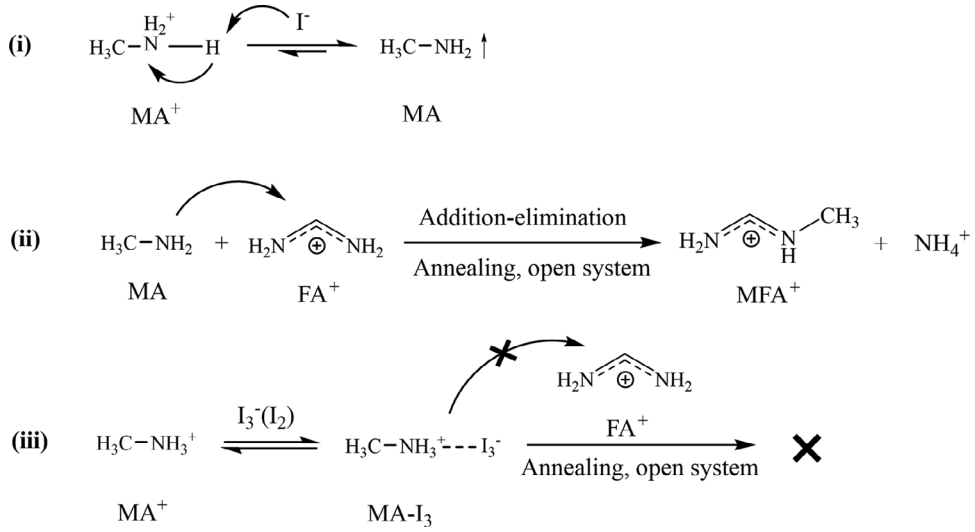

Scheme 1. The effect of iodine addition on precursor inks containing MA and FA upon annealing. i) The deprotonation of MA^+ and ii) the escape of volatile MA. The MA-FA side reaction between nucleophile MA and FA^+ to give MFA^+. iii) The strong interaction between I_3^- and MA^+ inhibits the MA-FA side reaction during annealing.

halide exchange within the organoammonium salts that is likely more pronounced in solution. Based on these observations, we speculate that I_2 does not interact with organoammonium cations directly, as shown in the case of MACl. However, in the presence of I^-, I_2 can be converted to I_3^- (or even polyiodides in the solid-state), where the loss of I_2 can be retarded through interaction with organoammonium cations. This interaction can be intuitively and macroscopically observed in Figure 2b. While mixing MACl and I_2 only results in a nonhomogeneous solid composition, mixing I_2 and methylammonium cations in the presence of I^- gives a liquid at room temperature, which have been identified as polyiodide compounds.[31] These ionic melts have been reported to assist the growth of halide perovskites in solid state or solution, and are relatively stable due to the gain of formation entropy.[31,32] We suspect that the formation of methylammonium polyiodides leads to a deferred release of I_2, as well as MA, during annealing.

The effect of I_2 addition in precursor solutions is further verified in thin film perovskites. **Figure 3a** shows the X-ray diffraction (XRD) patterns of as-coated perovskite films made from

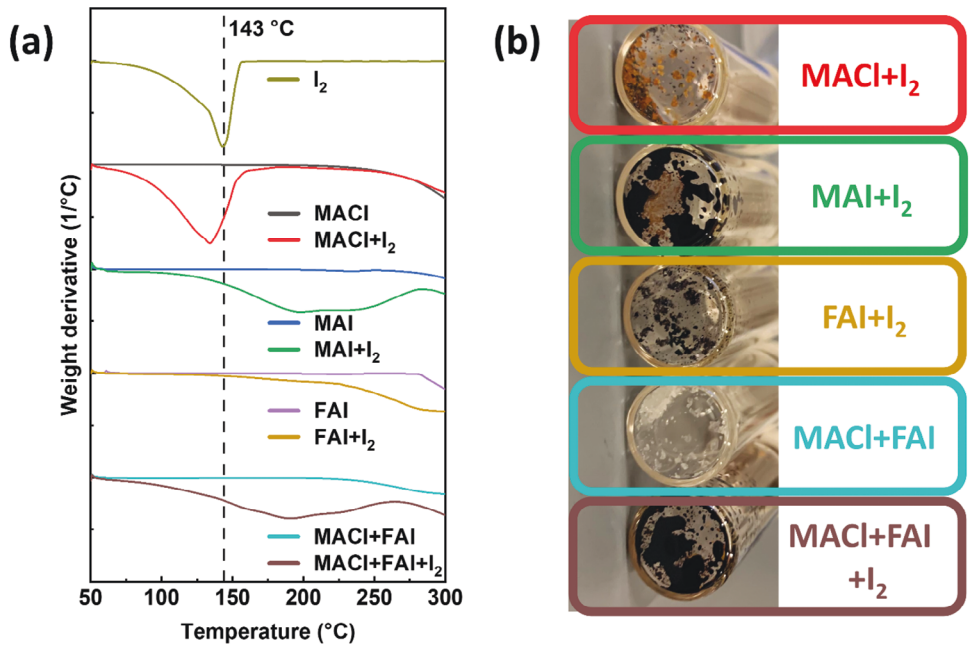

Figure 2. a) DTA curves of I_2 as well as solid mixtures of organoammonium halide salts with or without I_2. b) Photographs of 4 mL glass vials containing organoammonium halide salts with or without I_2.

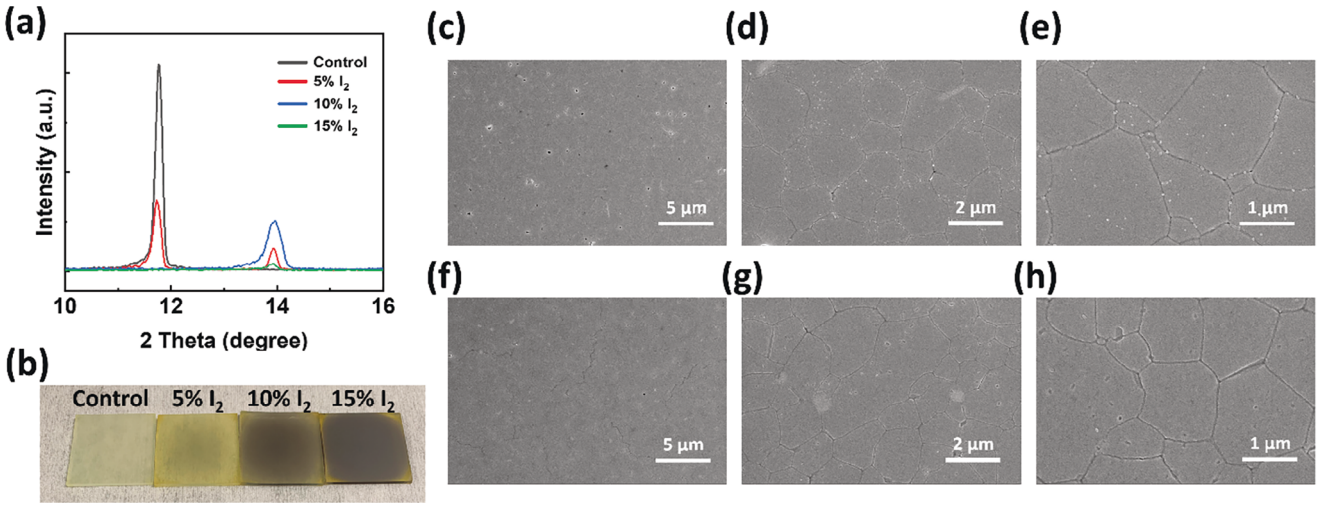

Figure 3. a) XRD patterns of as-coated perovskite thin films with different molar ratios of iodine in the precursor solution. b) As-coated perovskite thin films on 3 cm × 3 cm substrates turn black with increased iodine loading. c) SEM images at increasing magnification of perovskite buried interfaces for (c-e) control and f–h) with I_2 (5 mol%) after aging in N_2 at 85 °C for 1 week.

precursors with x mol% of I_2 (x = 5, 10, and 15) (denote as x% I_2) or without I_2 (control). It should be noted that there is an average 15 min aging at room temperature for each sample before XRD characterization. In contrast to the control that only displays a peak of δ-$FAPbI_3$ at 11.8°, that of 5% I_2 shows a largely suppressed peak of δ-$FAPbI_3$ and a new peak at 13.9° that is assigned to α-$FAPbI_3$. Interestingly, 10 or 15% I_2 loading results in films that only show the peak for α-$FAPbI_3$ at 13.9°, though the peak intensity is much lower for 15% I_2. Similar results can be seen in previous work where less volatile long-chain alkylammonium chloride additives were used.[10] This trend can also be seen in Figure 3b, where the colors of as-coated films gradually evolved from the yellow δ-$FAPbI_3$ to the black α-$FAPbI_3$ with increased I_2 loading. This observation is consistent with the fact that, with I_2 addition, MACl can be anchored within thin films longer during processing, and plays a more pivotal role in suppressing the undesired δ phase. Additionally, the minimal presence of side products such as MFA^+, which has been revealed to form trigonal $MFAPbI_3$ and prevent the formation of α-$FAPbI_3$, might also contribute to the abrupt conversion to α-$FAPbI_3$.[16] During the later stages of the annealing process, the solvent and MACl are less likely to escape from the layer. Solvents like DMSO possess high boiling points and have been linked to promoting the MA-FA side reaction due to proton transfer[29,30]; they can even be trapped at the bottom interface, undermining its stability.[33] With the accumulation of solvents and MACl, one can expect a larger degree of MA-FA side reaction at the bottom interface during annealing. Figure 3c–h shows scanning electron microscope (SEM) images of buried perovskite interfaces after aging. In the control sample (Figure 3c), there are voids of ≈200 nm in size, randomly distributed on the interface. These voids are surrounded by less conductive white regions, which could continue to expand and initiate degradation at the buried interface.[33] In addition, smaller particles with a size <20 nm reside preferentially at grain boundaries, as shown by images with higher magnification in Figure 3d,e. These white regions and small particles are already visible before aging as shown in Figure S7 (Supporting Information). Since trigonal $MFAPbI_3$ is not compatible with cubic α-$FAPbI_3$, we speculate that upon aging $MFAPbI_3$ preferentially forms and segregates into particles at grain boundaries. The formation of voids and particles will destabilize the buried interface and impede carrier collection. On the contrary, there are significantly fewer voids and particles on samples with 5% I_2 addition, as shown in Figure 3f–h, demonstrating the role of I_2 in mitigating the side reaction and enhancing interfacial stability at the buried interface. The top surfaces where the side reaction is less likely to occur exhibit no obvious difference as shown in Figure S8 (Supporting Information).

To investigate the impact of the addition of I_2 on PSCs, we fabricated devices using the pristine $FAPbI_3$ precursor solution and precursor solutions with various I_2 loadings. The devices comprised multiple layers: glass/fluorine-doped tin oxide (FTO)/SnO_2/perovskite/ 2,2′,7,7′-tetrakis[N,N-di(4-methoxyphenyl)amino]−9,9′-spirobifluorene (Spiro-OMeTAD)/Au. **Figure** 4a depicts the PCE distribution of 24 devices for each category. Although the amount of I_2 considerably exceeds prior attempts,[27,28] the addition of I_2 improved all three photovoltaic parameters: short-circuit current density (J_{sc}), open-circuit voltage (V_{oc}) and fill factor (FF) (Figure S9, Supporting Information). We attribute this improvement to reduced non-radiative recombination and improved charge collection resulting from the reduction of the undesired byproducts at the buried interface, as well as the prolonged presence of MACl during the annealing process. Figure 4b compares the current density-voltage (J-V) characteristics and forward and reverse bias sweeps for the best-performing PSCs fabricated with 5% I_2 (denoted as the target) and controls without I_2 addition. The J_{sc}, V_{oc}, FF, and PCE of the target were 25.4 mA cm^{-2}, 1.18 V, 84.2%, and 25.2%, respectively, while these metrics for the control were 25.2 mA cm^{-2}, 1.16 V, 82.4%, and 24.2%, respectively. The hysteresis in forward and reverse sweep was negligible at ≈0.2% absolute efficiency in both the control and the target. The integrated J_{sc} calculated from the external quantum efficiency (EQE) of the target (25.0 mA cm^{-2}) was higher than

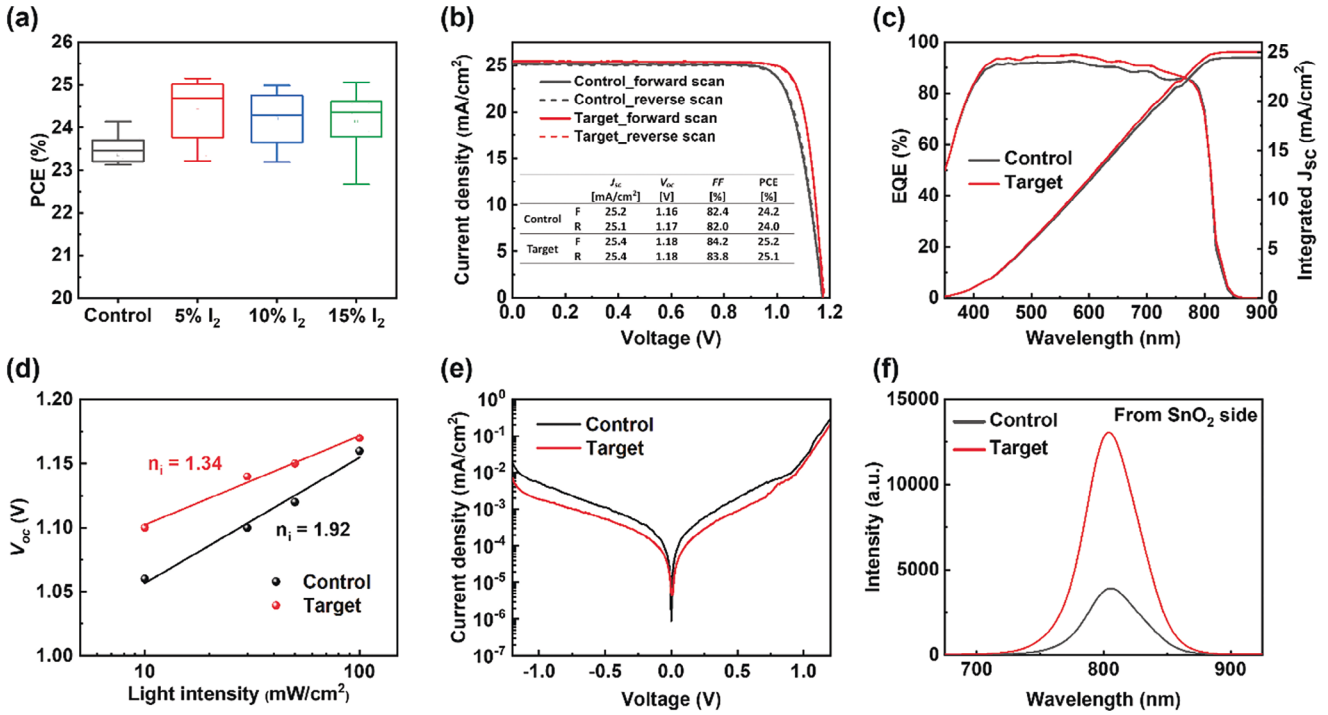

Figure 4. a) PCE distribution of 24 devices with various I_2 molar ratios in the precursor solutions (center line, median; small square, mean; box, 25–75% standard deviation; whiskers, outliers). b) *J–V* curves of the champion devices from the control and target. c) EQE spectra and integrated *Jsc* for the control and target. d) V_{oc} as a function of light intensity for the control and target. e) Dark *J-V* characteristics for the control and target. f) Steady-state PL spectra for the control and target perovskite thin film illuminated from the SnO_2 side (bottom side).

that of the control (24.4 mA cm^{-2}), which is consistent with the *J-V* characteristics (Figure 4c). In addition, cross-sectional SEM images of devices prepared with the control and the target show no significant differences (Figure S10, Supporting Information).

The improvement in V_{oc} and FF in the target device can be attributed to the mitigation of non-radiative recombination in the perovskite bulk or at interfaces. We measured V_{oc} as a function of light intensity to obtain the ideality factor (n_i), which reflects the degree of non-radiative recombination in the devices (Figure 4d). The n_i was calculated via

$$V_{oc} = n_i \left(k_B T/q\right) ln\left(I\right) + a \tag{1}$$

where k_B, T, q, I, and a represent the Boltzmann constant, temperature, elementary charge, light intensity, and a constant, respectively. The n_i value of the target (1.34) was closer to 1 than that of the control (1.92), indicating a more ideal diode behavior with less non-radiative recombination in the target device. We further conducted *J-V* characteristics of the control and the target in the dark to compare leakage current (Figure 4e). We can quantitatively assess leakage current and the shunt resistance by using the equation:

$$J = \frac{V}{R_{sh}} + J_r\left(e^{\frac{eV}{m_r k_B T}} - 1\right) + J_d\left(e^{\frac{eV}{m_d k_B T}} - 1\right) \tag{2}$$

where R_{sh}, J_r, J_d, m_r, and m_d are the shunt resistance, recombination current density, diffusion current density, and constants, respectively.[34] The calculated R_{sh}, J_r, and J_d are summarized in **Table 1**. The increased R_{sh} and decreased J_r are consistent with the improvement of FF of the target devices. Furthermore, by using the equation:

$$\ln\left(\mathrm{EQE}\right) = \mathrm{C} + \frac{hv}{E_u} \tag{3}$$

where C and hv are a constant and the photon energy, respectively, we derived the Urbach energy (E_u) (Figure S11, Supporting Information) of the control and the target from the EQE spectra (Figure 4c). The small E_u value indicates higher optoelectronic quality of the device. The E_u of the control was 15.2 meV, whereas it was 13.5 meV for the target.

We carried out steady-state photoluminescence (PL), with a 404 nm wavelength excitation source, from the Spiro-OMeTAD (top) and SnO_2 (bottom) sides. Due to the high absorption coefficient of the perovskite layer, a relatively short wavelength can only penetrate a few tens of nanometers into the perovskite layers. Therefore, the PL response from the bottom side can represent the buried interface, while the top side represents the perovskite

Table 1. R_{sh}, J_r, J_d derived from fitting dark *J-V* of PSCs in Figure 4e.

Condition	R_{sh} [MΩ cm^2]	J_r [mA cm^{-2}]	J_d [mA cm^{-2}]
Control	0.26	1.05×10^{-6}	1.49×10^{-11}
Target	0.49	8.16×10^{-7}	1.19×10^{-11}

surface.[29] While the PL intensity from both top and bottom sides of the target is higher than that of the control, the difference is more pronounced on the bottom side (Figure 4f; Figure S12, Supporting Information), suggesting significantly fewer interfacial defects at the bottom side for the target, attributed to the reduced formation of byproducts primarily occurring at the buried interface. The ideality factor, leakage current, Urbach energy, and PL were in good agreement with the V_{oc} and FF improvement in the target devices. Furthermore, we observed that the addition of I_2 into the precursor solution does not compromise stability of devices (Figure S13, Supporting Information) even if I_2 has generally been regarded to be detrimental to the stability of solid-state PSCs. This might be due to the fact that iodine will only stay in the precursor solution during crystallization, and can be fully removed upon annealing.

3. Conclusion

In summary, we demonstrate how I_2 additives alter the dynamics of MACl in $FAPbI_3$ precursor solutions, based on strong interaction between triiodide and organoammonium cations. We showed that the detrimental MA-FA side reaction during annealing can be largely mitigated with an enhanced perovskite bottom contact. In addition, owing to suppressed volatility, MACl can play a persistent role in facilitating the fast preferential growth of α-$FAPbI_3$ during annealing. The external I_2 strategy can further boost the device PCE to 25.2%, notably based on an already highly optimized recipe. Given that I_2 will not remain within the perovskite thin films after annealing, we expect that this strategy is compatible with other $FAPbI_3$ recipes featuring the use of MACl or other chloride-based alkylammonium additives.

Supporting Information

Supporting Information is available from the Wiley Online Library or from the author.

Acknowledgements

J.H. and J.W.A. contributed equally to this work. The authors acknowledge support provided by the United States Department of Energy's Office of Energy Efficiency and Renewable Energy (EERE) under their Solar Energy Technology Office (SETO) Award Number DE-EE0010503. The authors acknowledge the use of Princeton's Imaging and Analysis Center, which was partially supported through the Princeton Center for Complex Materials (PCCM), a National Science Foundation (NSF)-MRSEC program (DMR-2011750). H.M. acknowledges support from the National Research Foundation of Korea (RS-2023-00220077). J.H.N. acknowledges support provided by the National Research Foundation of Korea grant funded by the Korea Government (MSIP) (NRF-2022M3J1A1085279 and RS-2023-00208467) and the Korea Institute of Energy Technology Evaluation and Planning (KETEP) from the Ministry of Trade, Industry and Energy (20214000000680).

Conflict of Interest

The authors declare no conflict of interest.

Data Availability Statement

The data that support the findings of this study are available from the corresponding author upon reasonable request.

Keywords

iodine, methylammonium chloride, perovskite precursor solution

Received: January 30, 2024
Revised: March 19, 2024
Published online: April 13, 2024

[1] H. Min, D. Y. Lee, J. Kim, G. Kim, K. S. Lee, J. Kim, M. J. Paik, Y. K. Kim, K. S. Kim, M. G. Kim, T. J. Shin, I. S. Seok, *Nature* **2021**, *598*, 444.
[2] G. Kim, H. Min, K. S. Lee, D. Y. Lee, S. M. Yoon, S. I. Seok, *Science* **2020**, *370*, 108.
[3] M. Yang, Z. Li, M. O. Reese, O. G. Reid, D. H. Kim, S. Siol, T. R. Klein, Y. Yan, J. J. Berry, M. F. A. M. van Hest, K. Zhu, *Nat. Energy* **2017**, *2*, 17038.
[4] Z. Huang, Y. Bai, X. Huang, J. Li, Y. Wu, Y. Chen, K. Li, X. Niu, N. Li, G. Liu, Y. Zhang, H. Zai, Q. Chen, T. Lei, L. Wang, H. Zhou, *Nature* **2023**, *623*, 531.
[5] D.-K. Lee, N.-G. Park, *Appl. Phys. Rev.* **2023**, *10*, 011308.
[6] M. Kim, G.-H. Kim, T. K. Lee, I. W. Choi, H. W. Choi, Y. Jo, Y. J. Yoon, J. W. Kim, J. Lee, D. Huh, H. Lee, S. K. Kwak, J. Y. Kim, D. S. Kim, *Joule* **2019**, *3*, 2179.
[7] K. Odysseas Kosmatos, L. Theofylaktos, E. Giannakaki, D. Deligiannis, M. Konstantakou, T. Stergiopoulos, *Energy Environ. Mater.* **2019**, *2*, 79.
[8] L. Bi, Q. Fu, Z. Zeng, Y. Wang, F. R. Lin, Y. Cheng, H.-L. Yip, S. W. Tsang, A. K. Y. Jen, *J. Am. Chem. Soc.* **2023**, *145*, 5920.
[9] B. Charles, J. Dillon, O. J. Weber, M. S. Islam, M. T. Weller, *J. Mater. Chem. A* **2017**, *5*, 22495.
[10] J. Park, J. Kim, H.-S. Yun, M. J. Paik, E. Noh, H. J. Mun, M. G. Kim, T. J. Shin, S. I. Seok, *Nature* **2023**, *616*, 724.
[11] V. Valenzano, A. Cesari, F. Balzano, A. Milella, F. Fracassi, A. Listorti, G. Gigli, A. Rizzo, G. Uccello-Barretta, S. Colella, *Cell Rep. Phys. Sci.* **2021**, *2*, 100432.
[12] X. Wang, Y. Fan, L. Wang, C. Chen, Z. Li, R. Liu, H. Meng, Z. Shao, X. Du, H. Zhang, G. Cui, S. Pang, *Chem* **2020**, *6*, 1369.
[13] R. Liu, Z. Li, C. Chen, Y. Rao, X. Sun, L. Wang, X. Wang, Z. Zhou, T. Jiu, X. Guo, S. Frank Liu, S. Pang, *ACS Appl. Mater. Interfaces* **2020**, *12*, 35043.
[14] Z. Li, X. Wang, Z. Wang, Z. Shao, L. Hao, Y. Rao, C. Chen, D. Liu, Q. Zhao, X. Sun, C. Gao, B. Zhang, X. Wang, L. Wang, G. Cui, S. Pang, *Nat. Commun.* **2022**, *13*, 4417.
[15] Y. Zhang, Z. Xing, B. Fan, Z. Ni, F. Wang, X. Hu, Y. Chen, *Angew. Chem., Int. Ed.* **2023**, *62*, e202215799.
[16] L. Chen, M. Hu, S. Lee, J. Kim, Z.-Y. Zhao, S.-P. Han, M. S. Lah, S. I. Seok, *J. Am. Chem. Soc.* **2023**, *145*, 27900.
[17] S. Chen, X. Xiao, H. Gu, J. Huang, *Sci. Adv.* **2021**, *7*, eabe8130.
[18] Z. Liu, J. Hu, H. Jiao, L. Li, G. Zheng, Y. Chen, Y. Huang, Q. Zhang, C. Shen, Q. Chen, H. Zhou, *Adv. Mater.* **2017**, *29*, 1606774.
[19] D. Sun, Y. Gao, H. Raza, S. Liu, F. Ren, X. Hu, H. Wang, X. Meng, J. Wang, R. Chen, H. Sun, J. He, J. Zhou, Y. Pan, Z. Sun, W. Chen, Z. Liu, *Adv. Funct. Mater.* **2023**, *33*, 2303225.
[20] S. Wang, Y. Jiang, E. J. Juarez-Perez, L. K. Ono, Y. Qi, *Nat. Energy* **2016**, *2*, 16195.
[21] F. Fu, S. Pisoni, Q. Jeangros, J. Sastre-Pellicer, M. Kawecki, A. Paracchino, T. Moser, J. Werner, C. Andres, L. Duchêne, P. Fiala, M. Rawlence, S. Nicolay, C. Ballif, A. N. Tiwari, S. Buecheler, *Energy Environ. Sci.* **2019**, *12*, 3074.
[22] J. Hu, Z. Xu, T. L. Murrey, I. Pelczer, A. Kahn, J. Schwartz, B. P. Rand, *Adv. Mater.* **2023**, *35*, 2303373.
[23] S. Tan, I. Yavuz, M. H. Weber, T. Huang, C.-H. Chen, R. Wang, H.-C. Wang, J. H. Ko, S. Nuryyeva, J. Xue, Y. Zhao, K.-H. Wei, J.-W. Lee, Y. Yang, *Joule* **2020**, *4*, 2426.

[24] J. Hong, Z. Xu, D. Lungwitz, J. Scott, H. M. Johnson, Y.-H. Kim, A. Kahn, B. P. Rand, *ACS Energy Lett.* **2023**, *8*, 4984.
[25] Z. Xu, D. D. Astridge, R. A. Kerner, X. Zhong, J. Hu, J. Hong, J. A. Wisch, K. Zhu, J. J. Berry, A. Kahn, A. Sellinger, B. P. Rand, *J. Am. Chem. Soc.* **2023**, *145*, 11846.
[26] E. Bi, W. Tang, H. Chen, Y. Wang, J. Barbaud, T. Wu, W. Kong, P. Tu, H. Zhu, X. Zeng, J. He, S.-i. Kan, X. Yang, M. Grätzel, L. Han, *Joule* **2019**, *3*, 2748.
[27] W. S. Yang, B.-W. Park, E. H. Jung, N. J. Jeon, Y. C. Kim, D. U. Lee, S. S. Shin, J. Seo, E. K. Kim, J. H. Noh, S. I. Seok, *Science* **2017**, *356*, 1376.
[28] J. Kim, B.-w. Park, J. Baek, J. S. Yun, H.-W. Kwon, J. Seidel, H. Min, S. Coelho, S. Lim, S. Huang, K. Gaus, M. A. Green, T. J. Shin, A. W. Y. Ho-baillie, M. G. Kim, S. I. Seok, *J. Am. Chem. Soc.* **2020**, *142*, 6251.
[29] H. Min, J. Hu, Z. Xu, T. Liu, S.-U.-Z. Khan, K. Roh, Y.-L. Loo, B. P. Rand, *Adv. Mater.* **2022**, *34*, 2205309.
[30] S. Chen, X. Dai, S. Xu, H. Jiao, L. Zhao, J. Huang, *Science* **2021**, *373*, 902.
[31] A. A. Petrov, S. A. Fateev, Y. V. Zubavichus, P. V. Dorovatovskii, V. N. Khrustalev, I. A. Zvereva, A. V. Petrov, E. A. Goodilin, A. B. Tarasov, *J. Phys. Chem. Lett.* **2019**, *10*, 5776.
[32] A. A. Petrov, N. A. Belich, A. Y. Grishko, N. M. Stepanov, S. G. Dorofeev, E. G. Maksimov, A. V. Shevelkov, S. M. Zakeeruddin, M. Graetzel, A. B. Tarasov, E. A. Goodilin, *Mater. Horiz.* **2017**, *4*, 625.
[33] M. Wang, C. Fei, M. A. Uddin, J. Huang, *Sci. Adv.* **2022**, *8*, eabo5977.
[34] P. Liao, X. Zhao, G. Li, Y. Shen, M. Wang, *Nano-Micro Lett.* **2017**, *10*, 5.